Renewable Energy 180 (2021) 203–212

Contents lists available at ScienceDirect

Renewable Energy

journal homepage: www.elsevier.com/locate/renene

Patterned mesoporous TiO_2 microplates embedded in Nafion® membrane for high temperature/low relative humidity polymer electrolyte membrane fuel cell operation

Le Vu Nam [a, 1], Eunho Choi [b, 1], Segeun Jang [b, **], Sang Moon Kim [a, *]

[a] Department of Mechanical Engineering, Incheon National University, Incheon, Republic of Korea
[b] School of Mechanical Engineering, Kookmin University, Seoul, 02707, Republic of Korea

ARTICLE INFO

Article history:
Received 15 April 2021
Received in revised form
22 July 2021
Accepted 17 August 2021
Available online 21 August 2021

Keywords:
Polymer electrolyte membrane fuel cell
Patterned TiO_2 microplates
Composite membrane
High temperature
Low relative humidity

ABSTRACT

Incorporating inorganic fillers, such as SiO_2, TiO_2, and CeO_2, into the electrolyte membrane via the conventional casting and evaporation process is proved to intensify the water retention, thus improve the proton conductivity of the polymer electrolyte membrane (PEM) under high temperature. However, this approach does not dramatically enhance the performance of the composite membrane due to the issue of proton pathway reduction and fillers agglomeration. Herein, uniformly patterned mesoporous TiO_2 microplates (PTMPs) are successfully embedded on the anode side surface of the Nafion® membrane by using micro-hole stencil for spatially localizing the PTMPs and well-controlled ionomer spray technique. Interestingly, the membrane comprised of PTMPs with a diameter of ~50 μm and a height of ~5.2 μm exhibits the maximum power density by more than 35.2% compared to the reference Nafion® membrane with the same thickness (~25 μm) under 120 °C and relative humidity of 35% condition. The result indicates that suitably designed PTMPs-embedded Nafion® membrane is effective for improving the PEMFC performance under elevated temperature and low humidity conditions.

1. Introduction

Realizing a sustainable energy economy, along with environmental and economic benefits is the long-term goal of each nation in the world [1]. Recently, fuel cell technologies are particularly noteworthy since they have the capabilities to meet all major energy-policy priorities, such as the elimination of greenhouse gas pollution, high conversion efficiency, and long-term use [2,3]. Among kinds of fuel cells, polymer electrolyte membrane fuel cells (PEMFC) are a great candidate for transport, stationary, and portable power supplies due to their high power density, fast start-up, low operating temperature, and environmental friendliness [4–6]. Indeed, the PEMFC can directly convert chemical energy into electrical energy via electrochemical reaction, in which hydrogen is the main fuel and water is the only by-product [7,8]. As a key component in PEMFC, the polymer electrolyte membrane (PEM) significantly affects the PEMFC performance by enabling proton transport while separating fuels and oxidant gas [9,10]. The most commonly used PEM material is perfluorosulfonic acid-based Nafion® membrane owing to its good mechanical stability and high proton conductivity at standard PEMFC operating temperature (60–80 °C) [11,12]. Recent PEM researches have been focused on increasing proton conductivity, durability, as well as operating temperature [13,14]. It is supposed that relatively high temperature (>100 °C) is a favorable operating condition for PEMFC because of enhanced electrode kinetics, tolerance for CO catalyst poisoning, and most importantly, better water management [15–17]. However, under elevated temperature, the Nafion® membrane suffers from a severe decrease in proton conductivity due to low water absorption, which is known to be one of the limitations of the membrane [18,19]. To address this issue, until now, extensive studies have been conducted and the methodological approach by inserting hygroscopic inorganic materials (SiO_2, TiO_2, CeO_2, etc.) into the PEM showed a possibility to tackle the dehydration of the Nafion® membrane under elevated temperature [20,21]. Conventionally, one of the most common techniques for incorporating inorganic materials into the PEM is a simple casting method [22]. The embedded inorganic fillers in the ionic conductor have been

* Corresponding author.
** Corresponding author.
E-mail addresses: sjang@kookmin.ac.kr (S. Jang), ksm7852@inu.ac.kr (S.M. Kim).
[1] These authors contributed equally to this work.

https://doi.org/10.1016/j.renene.2021.08.062
0960-1481/

proved to effectively attain water molecules at high temperature by providing strong Coulombic attraction within the electrical double layer [23,24]. Nonetheless, the casting approach did not dramatically enhance the performance of the PEMFC under elevated temperature/low relative humidity operating condition, since it reduced proton pathways and promoted agglomeration of the fillers [25,26]. In a recent study, to avoid particle agglomeration, our group reported TiO_2/Nafion® composite membrane by transferring uniformly constructed mesoporous TiO_2 layers to the Nafion® membrane. This composite membrane was proven to be beneficial for improving the membrane electrode assembly (MEA) performance under elevated temperature/low humidity condition [23]. Nevertheless, the TiO_2 layer still acts as a barrier for the proton transport, although this method can resolve the agglomeration issue of the nano-sized inorganic fillers.

In this study, spatially and homogeneously patterned mesoporous TiO_2 microplates (PTMPs) comprised of nanoparticles and nanopores were successfully embedded onto the surface of the Nafion® membrane via a simple doctor blading process with a patterned micro-hole stencil and successive auto-spraying method of Nafion® ionomer. This approach not only resolved the coalescence issue of inorganic materials but also ensures the proton conductivity of the membrane by controlling the surface coverage of the PTMP layer. Moreover, the PTMPs with different morphologies were fabricated to compare the effects of each PTMPs for the mechanical behavior of the composite membrane and the electrochemical characteristics of the MEAs through conducting electrochemical impedance spectroscopy (EIS), electrochemical surface area (ECSA), and tensile test. The findings of these analyses revealed that the modified Nafion® membrane with well-designed PTMPs effectively improved the maximum power density of the MEA by more than 35.2% compared to that of the reference Nafion® MEA under elevated temperature/low relative humidity condition while maintaining proper mechanical properties.

2. Experimental section

2.1. Materials

Nafion® dispersion (Ew1000, D520), which contains 5 wt% of perfluorosulfonate resin and 95 wt% of 1-propanol/water/ethanol mixture (45:48.5:1.5 wt ratio), was purchased from Fuel cell store. For reducing the viscosity of the Nafion® dispersion to make a proper solution for applying spraying method, the received Nafion® dispersion was further diluted to 1 wt% while keeping the composition ratio of the 1-propanol/water/ethanol mixture. The other materials including Nafion® membrane (NRE-211, Chemours, United States), UV-curable polymer (MINS PUA 311RM, Changsung sheet, Korea), TiO_2 paste (18NR-T, 20 nm size, Dyesol Ltd, Australia), PDMS (Sylgard 184, Dow Corning, United States) were used as received.

2.2. Preparation of micro PDMS molds

The PDMS molds with micro-pillar patterns (50 μm and 500 μm) were prepared via soft lithography using micro-hole patterned silicon masters (50 μm and 500 μm) fabricated by photolithography and deep reactive ion etching. The mixed solution of PDMS elastomer base resin and curing agent (10:1 w/w) was poured onto the patterned silicon master and thermally cured at 70 °C for 2 h. Then, the replicated PDMS mold detached from the silicon master.

2.3. Preparation of PUA stencils with micro apertures

1 mL of UV-curable PUA resin was dispensed onto the PDMS mold with micro-pillars and a flat PDMS mold was covered onto them (Fig. 1a). Next, the sandwich-like assembly was irradiated under UV light (F8T5BL, $\lambda = 352$ nm, SANKYO DENKI) with the UV intensity of 20 W cm^{-2} for 1 min to make the PUA stencil with micro-aperture (Fig. 1b). The cured PUA stencil (3 cm × 3 cm) was detached from the PDMS molds and placed on the glass substrate (S9213, Matsunami, Japan) (Fig. 1c and d). Three PUA stencils of 20 μm thickness with different aperture sizes of 50 μm (Fig. 2a), 500 μm (Fig. 2b), and blank flat square (Fig. 2c) were prepared.

2.4. Fabrication of patterned mesoporous TiO_2 microplates (PTMPs)

The TiO_2 paste was directly dispensed onto the PUA stencil and inserted into the holes of the stencil by the simple doctor blading method (Fig. 1e). The PUA stencil coated TiO_2 paste on glass substrate was put on a hot plate at 100 °C for 1 h to evaporate the residual solvent of the paste and the PUA stencil was peeled off (Fig. 1f). Then, the sintering process was performed in a furnace (FB1310M, Thermo Scientific, United States) above 500 °C for 1 h to completely remove the polymeric binder in the paste and accelerate the necking of TiO_2 nanoparticles (Fig. 1g). Finally, each three of the mesoporous PTMPs made from different dimensions of PUA stencil was designated to PTMPs 50 (TiO_2 microplates with a diameter of 50 μm), PTMPs 500 (TiO_2 microplates with a diameter of 500 μm), and FT (flat layer of TiO_2).

2.5. Fabrication of PTMPs-embedded Nafion® membrane

The diluted Nafion® ionomer solution was sprayed onto the PTMPs on a glass substrate (Fig. 1h) to make PTMPs-embedded membrane, and onto the bare glass to make the bare Nafion® membrane (Fig. 2d, h). For constructing the membrane by a spraying method, we utilized an auto-spray machine to spray the ionomer solution by setting a serpentine path with an area of 59 × 59 mm^2 and an interval length of 1 mm, and the spray path was rotated by 90° to counter-clockwise direction after every single serpentine spray path. Then, four times spraying following the single serpentine path consists of one cycle. After every single spray cycle, the center of the spray nozzle was moved to half-width of the interval length (0.5 mm) to achieve better uniformity of the membrane. This spray cycle was repeated until obtaining the target thickness. The feed rate and flow rate were set to 6 cm/s and 1 ml min^{-1}, respectively. After that, the Nafion® film-coated glass substrate was heat-treated for 12 h at 80 °C in an oven to remove the residual solvent and further thermal annealing process was carryout at 130 °C for 2 h to improve the membrane properties [27,28]. All membranes were fabricated to have the same thickness as the commercial NRE-211 membrane (25 μm). Next, the membranes were carefully detached from the glass substrate and soaked into a 0.5 M sulfuric acid solution at 70 °C in 2 h for reprotonation of the membrane [29] and rinsed several times with DI water. Finally, five membranes were prepared and designated as PTMPs 50 membrane, PTMPs 500 membrane, FT membrane, Bare membrane, and NRE-211 membrane (Fig. 2e–i).

2.6. Preparation of membrane electrode assembly (MEA)

The carbon-supported Pt catalyst (40.0 wt% Pt, Johnson Matthey, United Kingdom), 5 wt% Nafion® ionomer solution, DI water, and isopropyl alcohol were mixed and further treated with ultrasonication for 20 min. The platinum loading and ionomer to carbon ratio were set to 0.2 mg/cm^2 and 0.5 on both anode and cathode sides, and the active area of all the MEAs was 5.0 cm^2. The five constructed MEAs have been denoted as follows: PTMPs 50 MEA; PTMPs 500 MEA; FT MEA; Bare MEA; and NRE-211 MEA.

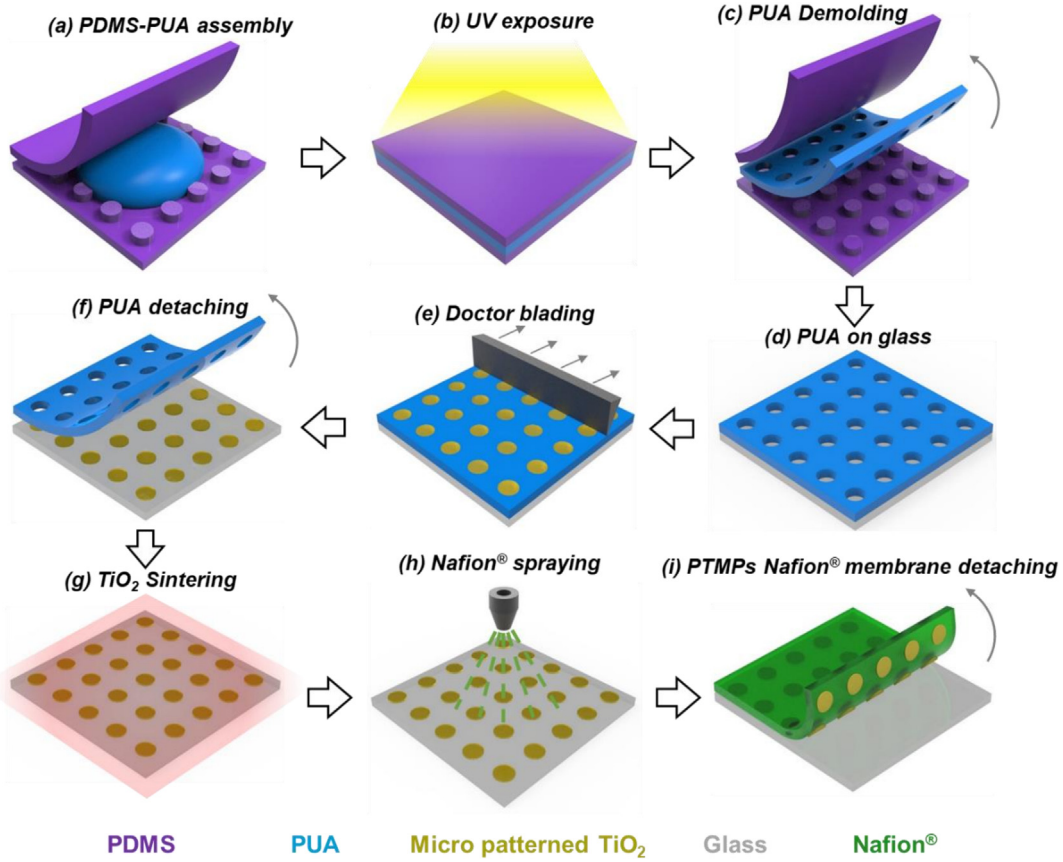

Fig. 1. Schematic illustrations of the fabrication process of PTMPs embedded in Nafion® membrane. (a) Sandwich-like assembly of micro-dots PDMS mold, PUA pre-polymer, and flat PDMS mold. (b) PUA curing under UV-light. (c) Demolding cured PUA stencil. (d) Attaching PUA stencil onto the glass substrate. (e) Doctor blading for TiO_2 paste on PUA mask. (f) Detaching PUA stencil after drying TiO_2 paste. (g) Sintering PTMPs structure. (h) Spraying Nafion® solution. (i) Detaching PTMPs Nafion® membrane from the substrate.

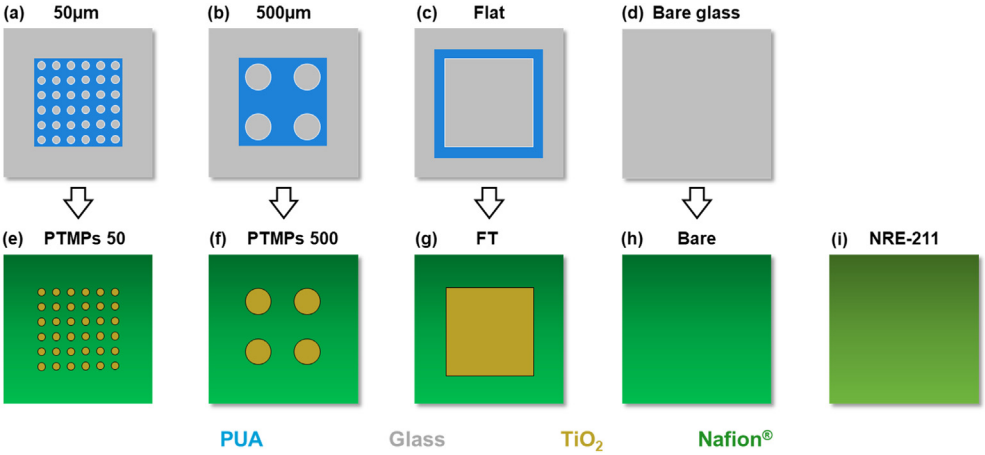

Fig. 2. (a–d) Schematic illustrations of prepared PUA stencils on the glass substrates: (a) 50 μm diameter hole pattern PUA mask, (b) 500 μm diameter hole pattern PUA mask, (c) blank square PUA mask, and (d) Bare glass substrate with no mask. (e–i) Schematic illustrations of prepared membranes: (e) PTMPs 50 membrane, (f) PTMPs 500 membrane, (g) FT membrane, (h) Bare membrane, and (i) commercial NRE-211 membrane.

2.7. Single-cell assembly

The prepared MEA was placed between two GDLs (SGL 35BC, Sigracet), two bipolar plates with a serpentine channel (width: 1 mm), and Teflon gaskets (290 μm thickness, CNL Energy, Korea) as shown in Fig. S1. This single-cell assembly was fastened by eight bolts with applying a torque of 70 ft-lb.

2.8. Electrochemical characterization

The device performances of the prepared MEAs were measured by a standard PEMFC test station (CNL, Korea). To investigate the electrochemical characteristics of the MEAs under elevated temperature and low relative humidity conditions, operating conditions of single cells were set to be varied from 100% RH @80 °C to

35% RH @120 °C. The flow rates of the H_2 and air were fixed at 150 mL min^{-1} and 80 mL min^{-1} to the anode and cathode, respectively. An impedance analyzer (HCP-803, Biologic, France) was used to investigate the EIS spectra and calculate the ECSA of each MEA. The EIS was measured at 0.6 V with an amplitude of 5 mV in the range of frequency from 0.1 Hz to 15 kHz. To determine the ECSA of the cathode electrode, Cyclic voltammetry (CV) was conducted at room temperature by supplying humidified N_2 (200 mL min^{-1}) and H_2 (200 mL min^{-1}) to the cathode (working electrode) and the anode (counter and reference electrode).

2.9. Physical characterization

A field-emission scanning electron microscopy (FE-SEM) (HITACHI SU-5000, Japan) with energy-dispersive X-ray spectroscopy (EDS) was used to study the morphological and compositional characteristics of the prepared membranes. The mechanical properties of the membranes were measured at room temperature by a universal test machine (3340, Instron Corp, United States) with a strain rate of 5 mm/min and a sample size of 10 mm width × 20 mm length.

3. Results and discussion

3.1. Morphology analysis

The morphological characteristics of the fabricated PTMPs 50/500 membranes, FT membrane, and Bare membrane were confirmed through observation of digital camera images and optical microscope images as shown in Fig. 3. In the optical microscope images, surface cracks were observed in the mesoporous PTMPs due to the volume shrinkage of the TiO_2 paste during the sintering process. However, this is not considered as the defect in this study since the cracks can be advantageous for ensuring proton conductivity compared to the flat TiO_2 film if the void spaces of the cracks are well filled with Nafion® ionomer during the spraying process. To further figure out how the mesoporous PTMPs were embedded in the surface of the composite membranes, cross-sectional SEM images were obtained in Fig. 4. While the initial thickness of the TiO_2 structures on PUA stencil after doctor blading was 20 μm, which is confirmed from the observation of the TiO_2 paste filling out the apertures of the PUA stencil (Figs. S2, S3, and S4), the thickness of both PTMPs 50 and 500 was reduced to be approximately 5.2 μm regardless of the pattern size of PTMPs (Fig. 4a–c). This reduction is attributed to the drying and sintering process at which the TiO_2 paste residues such as solvents and polymer binder were removed, and only the sintered TiO_2 structure remained. Interestingly, when the pattern diameter reduction of each PTMP after the sintering process was compared, there seemed no changes in the diameter of PTMPs before and after the process. The result indicates that the patterned TiO_2 paste layer was dominantly contracted to the through-plane direction and there was an insignificant change in in-plane direction during the sintering process. In addition, the TiO_2 surface coverage ratio and TiO_2 volume ratio of PTMP 50 and PTMP 500 membranes were estimated the same with the value of ~19.6% and ~3.5%, respectively (Fig. S5), which means the same amount of TiO_2 filler in PTMP 50 and PTMP 500 are loaded in both cases. Indeed, the PTMPs were deeply embedded inside the Nafion® membrane surface as expected, and the interface between the PTMPs and Nafion® membrane was well interconnected without void space at the interface. Moreover, the thickness of all the spray-based membranes was uniform and similar to the NRE-211 membrane, therefore we can compare the performances of the MEAs with the prepared membranes excluding the thickness effect (i.e. ohmic resistance), and solely figure out the role of the mesoporous PTMPs incorporated into the membrane. After constructing MEAs, the morphology of the PTMPs 50 MEA, PTMPs 500 MEA, and FT MEA was characterized by cross-sectional SEM images, and the elemental distribution was further analyzed by EDS mapping as shown in Fig. 5. In EDS mapping images, each Ti and F element clearly exhibited the constructed mesoporous TiO_2 structure and perfluorinated Nafon®, respectively.

3.2. Membrane properties

After confirmation of the morphological characteristics, mechanical properties of the prepared membranes were investigated because these are critical factors for determining the durability of the PEM during repeated wet/dry operational condition of the PEMFC. Stress-strain behaviors of the membranes are displayed in Fig. 6a, and the measured mechanical properties including tensile strength, elongation to break, and Young's modulus are plotted in Fig. 6b–d. The Bare membrane fabricated through spray process showed higher tensile strength than the commercial NRE-211

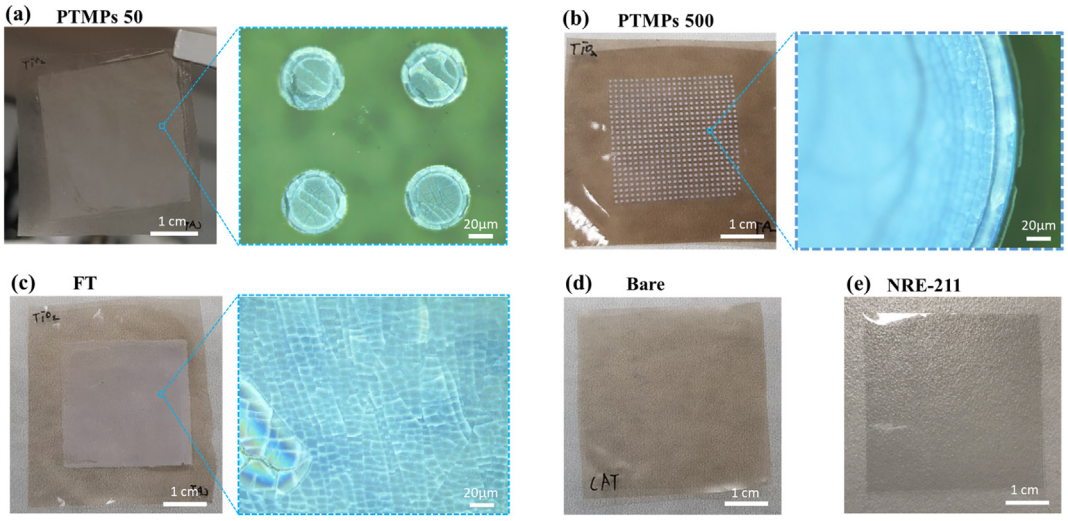

Fig. 3. Physical observation with digital camera and optical microscopy for (a) PTMPs 50 membrane, (b) PTMPs 500 membrane, (c) FT membrane, (d) Bare membrane, and (e) NRE-211 membrane.

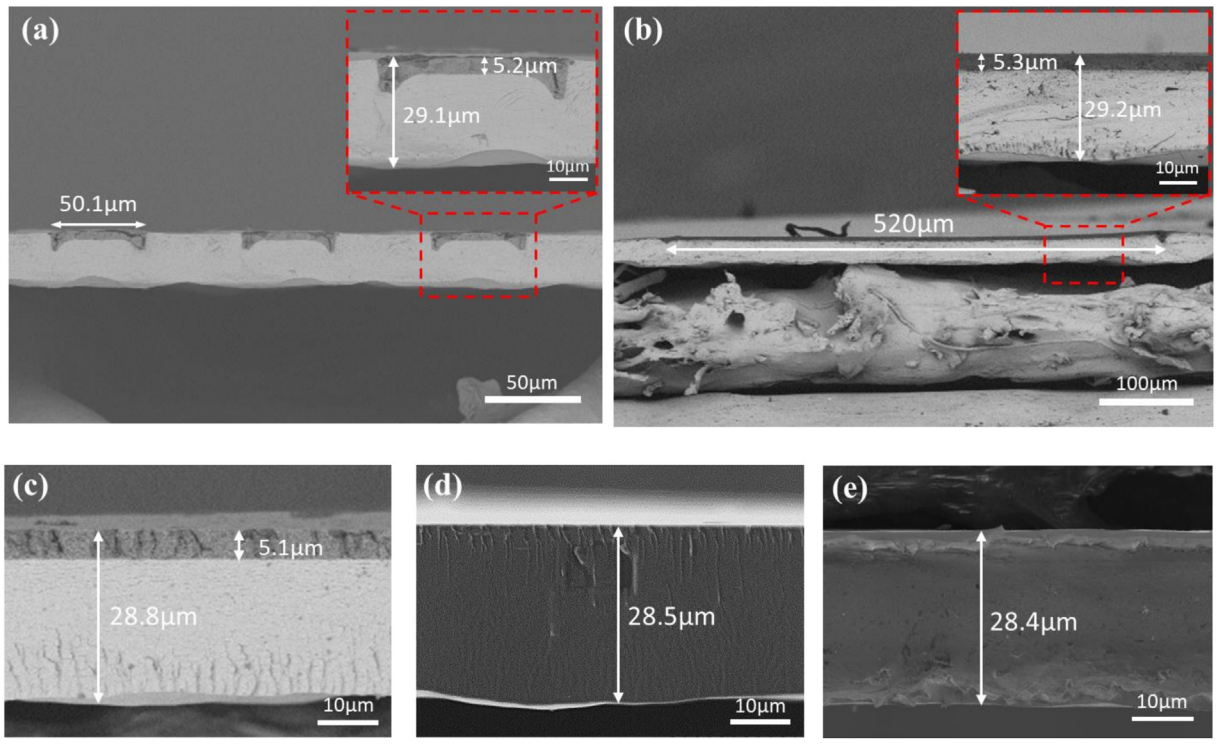

Fig. 4. Cross-sectional SEM images of (a) PTMPs 50 membrane, (b) PTMPs 500 membrane, (c) FT membrane, (d) Bare membrane, and (e) NRE-211 membrane.

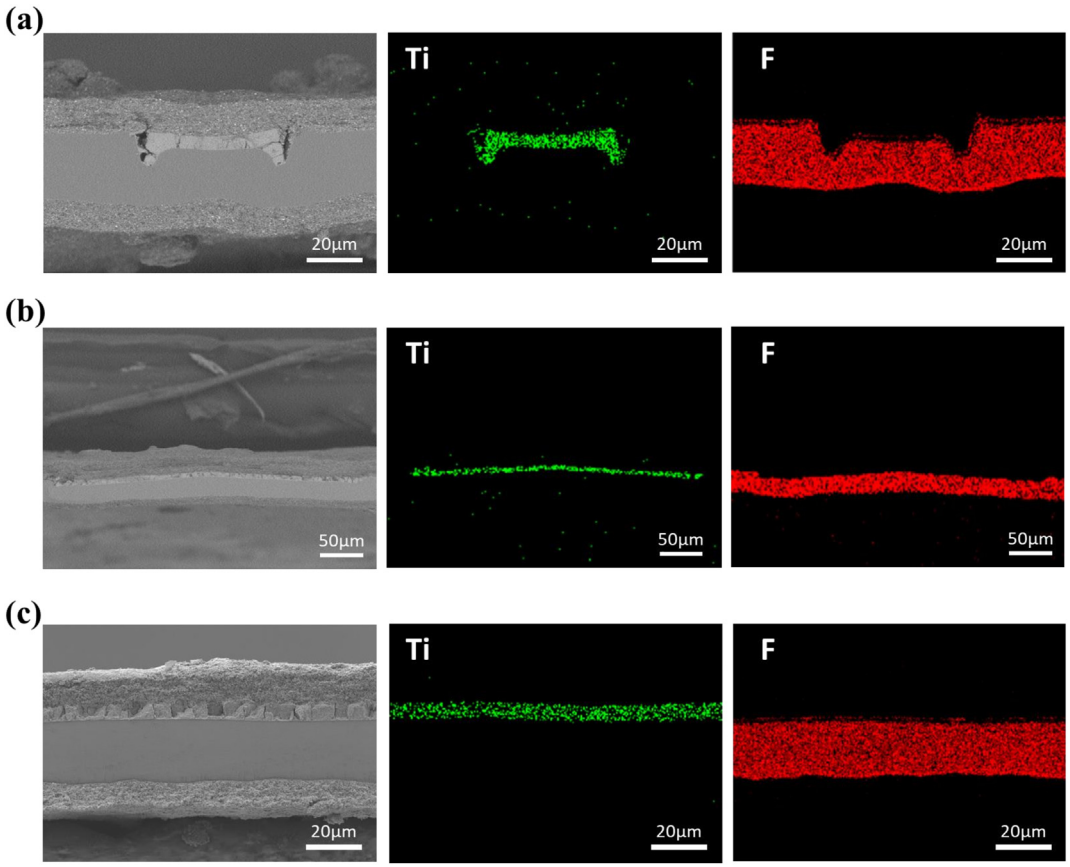

Fig. 5. Cross-sectional SEM images and EDS mapping of Ti and F of prepared MEAs: (a) PTMPs 50 MEA, (b) PTMPs 500 MEA, and (c) FT MEA.

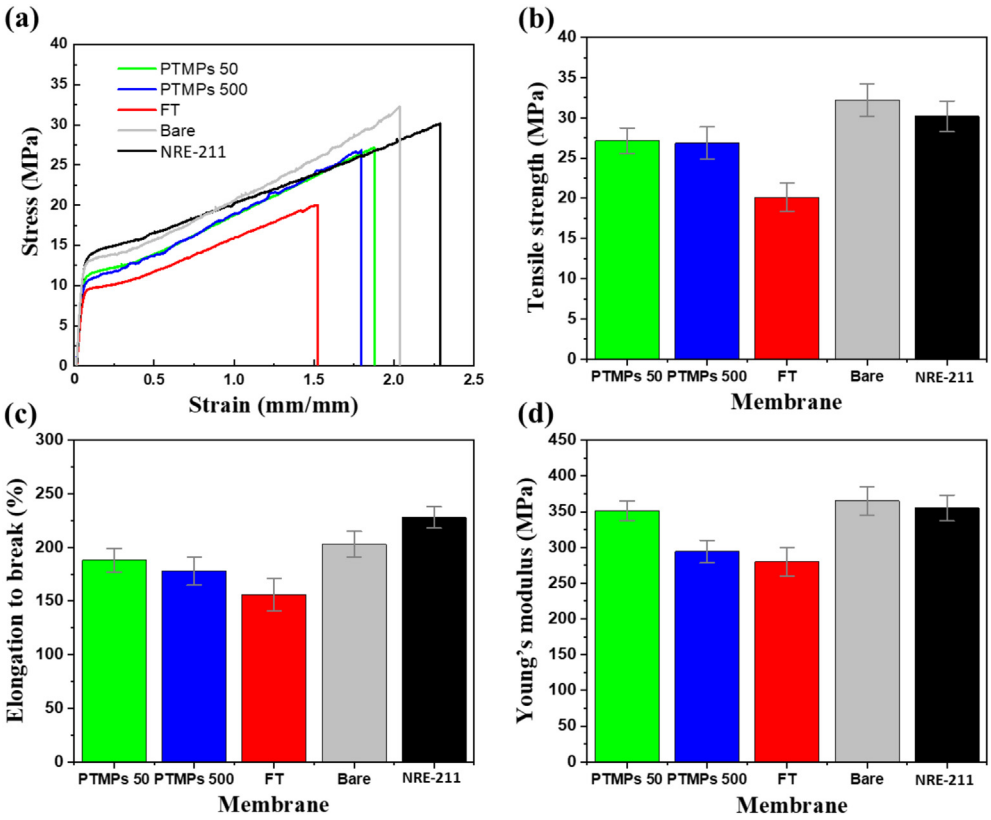

Fig. 6. Mechanical strength properties of the prepared membranes: (a) stress-strain curves, (b) tensile strength, (c) elongation to break, and (d) Young's modulus.

membrane, which can be ascribed to the well-designed spraying-based membrane fabrication process and additional thermal annealing process driven reinforcement of the membrane [27,28]. Interestingly, when three TiO_2-embedded membranes (PTMPs 50, PTMPs 500, and FT membrane) were compared, the mechanical strength got lowered as the TiO_2 coverage of the surface increased. This may come from the heterogeneous composition of the composite membrane resulted in stress mismatch in the cross-sectional area during the stretching process and it initiated fracture of the membrane. As a result, the FT membrane with the entirely covered TiO_2 layer at one side showed the lowest tensile strength of 20.15 MPa and elongation to break of 156%. This implies that the spatially patterned mesoporous PTMPs are advantageous for maintaining sufficient mechanical properties of the membrane as well as securing more proton pathways. Additionally, to investigate the mesoporous PTMPs induced hydration effect on the membrane, we performed further characterization of the membrane properties including length change, thickness change, water uptake, and in-plane proton conductivity. As shown in Table S1, the PTMPs 50 membrane showed a much higher water uptake capacity of 32.6% compared to the reference NRE-211 (22.0%) and Bare (20.5%) membranes at 80 °C with having larger volume changes driven by increased length and thickness changes. In the case of the proton conductivity (Fig. S6), the PTMPs 50 membrane showed comparable proton conductivity of about 0.278 S/cm at the condition of 100% RH @80 °C compared to that of the reference NRE-211 (0.281 S/cm). However, it showed over 47% higher conductivity (0.0419 S/cm) relative to the reference NRE-211 (0.0284 S/cm) in the condition of 35% RH @120 °C where proton transport is limited due to the severe dehydration of the Nafion® matrix. The conductivity differences between those membranes were getting increased as the temperature increases and the relative humidity decreases, and it can be ascribed to the high water-retention effect of the PTMPs with strong Coulombic attraction to water molecules within the electrical double layer. The experimental details were described in supporting information.

3.3. Electrochemical analysis

To elucidate the impact of PTMPs-embedded MEAs on PEMFC performance under elevated temperature and low humidity conditions, the electrochemical single-cell tests were conducted on all the prepared MEAs (see details in the **Experimental section**). During the MEA preparation, the TiO_2 structured side of the membrane was chosen to be the anode side because, under elevated temperature/low relative humidity condition, dehydration of the membrane at the anode is more severe than that of the cathode where the water is generated from the oxygen reduction reaction [23]. The measured polarization curves of the prepared MEAs under four different operating conditions (100% RH and 50% RH @80 °C, 51% RH @105 °C, and 35% RH @120 °C) and the corresponded EIS results are showed in Figs. 7 and 8, respectively, and each key parameter values are summarized in Tables 1 and 2. Firstly, in the case of Bare MEA made from spray-based method, it exhibited the comparable I–V characteristics (Fig. 7 and Table 1) and analogous values of the ohmic resistance (R_{ohm}) and the kinetic loss (R_{ct}) from the EIS spectra (Fig. 8 and Table 2) under all testing conditions compared to those of the reference NRE-211 MEA. The results signified that the laboratory-made membrane with a well-controlled auto-spray method showed similar mechanical and electrochemical properties relative to those of the commercial Nafion® NRE-211 membrane with the same thickness. On the contrary, the FT MEA exhibited extremely inferior performances under all operating conditions, which indicated that the flat TiO_2

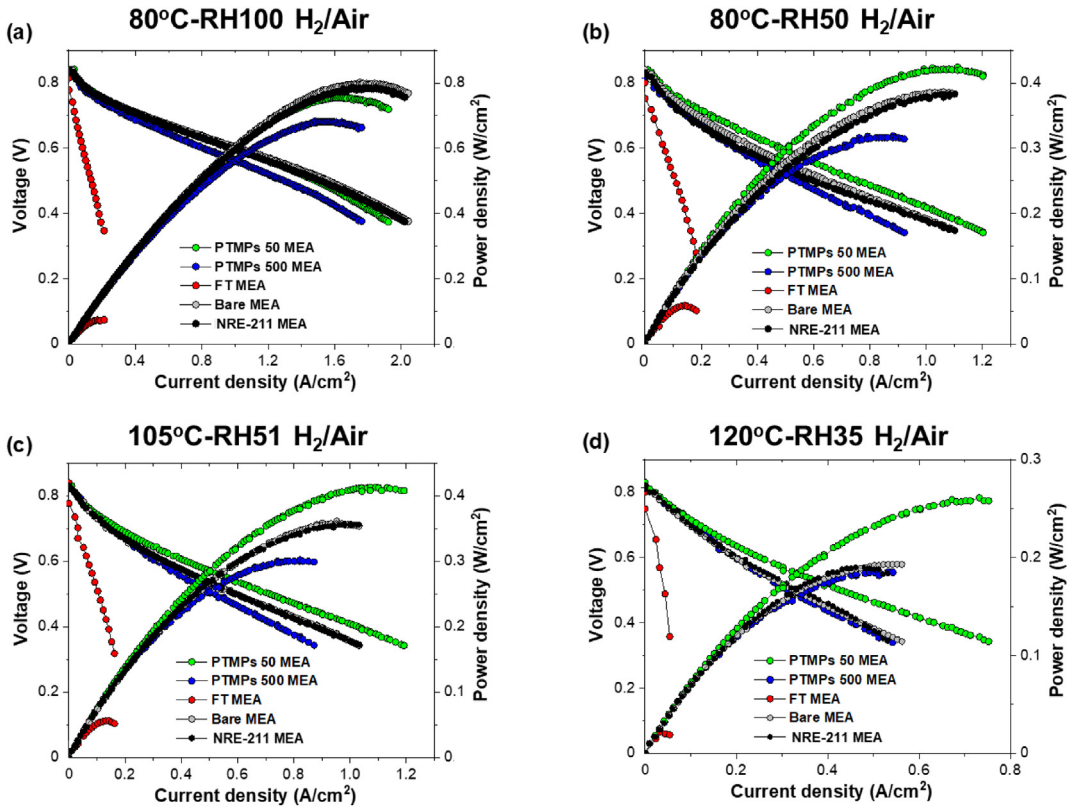

Fig. 7. Polarization curves of prepared MEAs under different operating conditions at (a) 80 °C with fully humidified (100% RH) H_2/Air, (b) 80 °C with partially humidified (50% RH) H_2/Air, (c) 105 °C with partially humidified (51% RH) H_2/Air, and (d) 120 °C with low humidified (35% RH) H_2/Air.

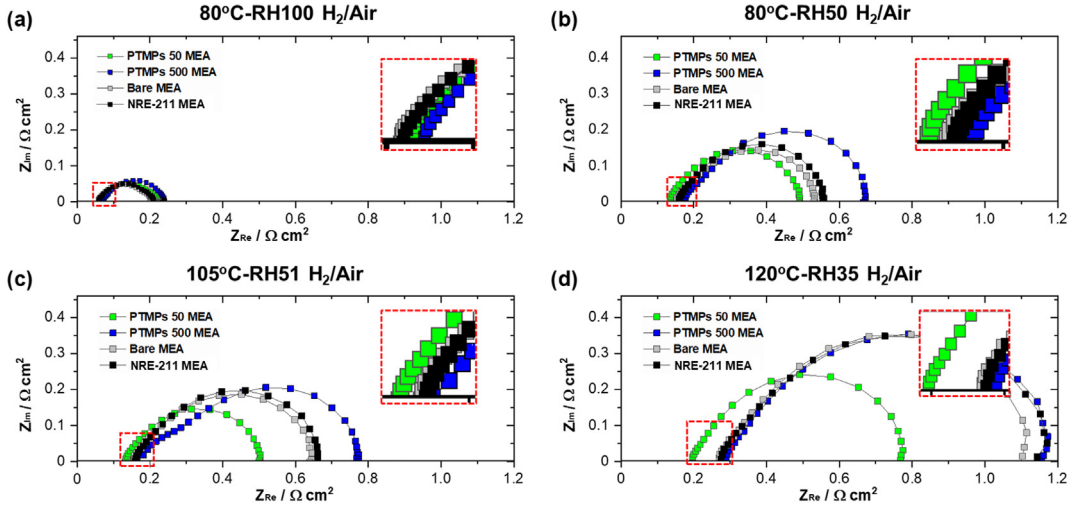

Fig. 8. Electrochemical analysis at 0.6 V under different operating conditions at (a) 80 °C with fully humidified (100% RH) H_2/Air, (b) 80 °C with partially humidified (50% RH) H_2/Air, (c) 105 °C with partially humidified (51% RH) H_2/Air, and (d) 120 °C with low humidified (35% RH) H_2/Air.

layer with a thickness of ~5.2 μm, which covered the entire surface of the anode side of the membrane severely hindered proton transport across the membrane. Therefore, spatially localizing the TiO_2 layer via the construction of the PTMPs is a highly desirable approach to effectively alleviate the loss of proton conductivity in the membrane by securing more proton pathways. In the case of the PTMPs membranes, the PTMPs covered region is responsible for increasing the water retention for humidifying the membrane in the condition of elevated temperature and low relative humidity while the other region (PTMPs-free region), where the electrochemical reaction occurs most efficiently, manages to provide proton transport pathways by contacting with electrode layer. By using the patterned micro-hole array stencil, the surface coverage, geometry, and quantity of desired PTMPs have been easily controlled. When comparing the performances of the MEAs with different geometry of the PTMPs (PTMPs 500 and 50), the PTMPs 500 MEA exhibited much lower fuel cell performances under all operating conditions than those of the PTMPs 50 MEA. Even if the

Table 1
Current density at 0.6 V and maximum power density of the samples from the single-cell polarization curves.

	PTMPs 50 MEA		PTMPs 500 MEA		Bare MEA		NRE-211 MEA	
	Current density at 0.6 V (mA/cm^2)	Maximum power density (mW/cm^2)	Current density at 0.6 V (mA/cm^2)	Maximum power density (mW/cm^2)	Current density at 0.6 V (mA/cm^2)	Maximum power density (mW/cm^2)	Current density at 0.6 V (mA/cm^2)	Maximum power density (mW/cm^2)
80°C-100% RH	992 (−1%)	755 (−5.7%)	812 (−18.9%)	679 (−15.2%)	1002 (0%)	801 (0%)	972 (−3.0%)	786 (−2.0%)
80°C-50% RH	482 (+26.2%)	424 (+9.8%)	316 (−17.3%)	319 (−17.4%)	382 (0%)	386 (0%)	352 (−7.8%)	383 (−0.8%)
105°C-51% RH	422 (+19.9%)	413 (+14.4%)	305 (−13.4%)	302 (−16.3%)	352 (0%)	361 (0%)	342 (−2.8%)	356 (−1.4%)
120°C-35% RH	252 (+31.3%)	261 (+35.2%)	190 (−1.0%)	185 (−4.1%)	192 (0%)	193 (0%)	190 (−1.0%)	190 (−1.6%)

Percentages: the ratio compared to the reference Bare MEA.

Table 2
EIS fitted values at 0.6 V.

	PTMPs 50 MEA		PTMPs 500 MEA		Bare MEA		NRE-211 MEA	
	R_{ohm} (Ω cm^2)	R_{ct} (Ω cm^2)	R_{ohm} (Ω cm^2)	R_{ct} (Ω cm^2)	R_{ohm} (Ω cm^2)	R_{ct} (Ω cm^2)	R_{ohm} (Ω cm^2)	R_{ct} (Ω cm^2)
80°C-100%RH	0.071 (+20.7%)	0.1705 (+14.7%)	0.0781 (+32.8%)	0.1743 (+17.2%)	0.0588 (0%)	0.1487 (0%)	0.0583 (−0.9%)	0.1517 (+2.0%)
80°C-50%RH	0.1316 (−13.8%)	0.3641 (−4.2%)	0.1745 (+14.4%)	0.4866 (+28.1%)	0.1526 (0%)	0.3799 (0%)	0.1571 (+2.9%)	0.3967 (+4.4%)
105°C-51%RH	0.1342 (−15.3%)	0.3674 (−24.7%)	0.1814 (+14.5%)	0.5926 (+21.4%)	0.1584 (0%)	0.4881 (0%)	0.1607 (+1.5%)	0.5001 (+2.5%)
120°C-35%RH	0.1961 (−27.4%)	0.5718 (−31.4%)	0.2828 (+4.7%)	0.8751 (+5.0%)	0.2701 (0%)	0.8332 (0%)	0.2753 (+1.9%)	0.8681 (+4.2%)

Percentages: the ratio compared to the reference Bare MEA.

thickness of the PTMPs is similar, it seems that the water retention feature of the composite membrane with laterally larger-sized PTMPs is overshadowed by the much-reduced proton conductivity. This is because the bigger the diameter of PTMP, the larger the proton pathway restrictive area exists on the surface of the membrane. Therefore, there would be a restriction for the selection of the size of the PTMP as illustrated in Fig. S7, and the result of the lower performances of the 500 MEA than the 50 MEA can be explained. When it comes to the PTMPs 50 MEA, under 100% RH @80 °C, the maximum power density was slightly 5.7% lower than that of the Bare MEA. This is because the adverse effect of insertion of non-ionic conducting material into the membrane is larger than the hygroscopic effect under fully humidified operating condition. However, as the operating temperature increased and the relative humidity reduced, the performance of the PTMPs 50 MEA was prominently increased compared to other MEAs with commercial NRE-211 and spray-based Bare membranes since the improved water retention features of the PTMPs effectively alleviated the dehydration of the membrane. The maximum power density of PTMPs 50 MEA was found to be 9.8% greater than that of Bare MEA under 50% RH @80 °C condition and it was much increased by 14.4% at the temperature of 105 °C with the same relative humidity condition. Additionally, under the condition of 50% RH@120 °C with keeping the same relative humidity, the PTMPs showed the improved maximum power density and current density at 0.6 V about 19.7% and 16.7% relative to those of the Bare MEA (Fig. S8 and Table S2). Notably, at 35% RH @120 °C operating condition, the maximum power density and current density at 0.6 V of the PTMPs 50 MEA were remarkably increased by more than 35.2% and 31.3% compared to those of the Bare MEA, respectively. This is because the high Coulombic attraction for the water molecules of the TiO_2 strongly reduced evaporation of the water at the temperature above the water boiling point [23]. The advantage of the composite membrane with PTMPs at high temperature/low relative humidity condition was further confirmed by the EIS measurements as shown in Figs. 8 and S9 and Tables 2 and S3. While the R_{ohm} and the R_{ct} of the PTMPs 50 MEA (0.071 Ωcm^2 and 0.1705 Ωcm^2) was higher than those of the Bare MEA (0.0588 Ωcm^2 and 0.1487 Ωcm^2) under fully humidified 100% RH @80 °C condition, at the harsh condition of 35% RH @120 °C, they were notably reduced by 27.4% and 31.4%, respectively, compared to those of the Bare MEA (0.2701 Ωcm^2/ 0.8332 Ωcm^2) with the aid of the water retention capability of the PTMPs inside the membrane. The changes of the R_{ohm} of the MEAs with varying operation conditions were plotted in Fig. S10, and it exhibited the effect of PTMPs 50 for reducing ohmic resistance (i.e. improving proton conductivity) by hydrating the Nafion® membrane at the elevated temperature and low RH condition. And this showed a good agreement with the results of improved water uptake and proton conductivity of the PTMPs 50 membrane (Table S1 and Fig. S6).

After analysis of I–V characteristics for each MEA, the ECSA values of the MEAs were obtained from the CV measurements (Fig. S11). As shown in Table 3, all prepared samples exhibited almost similar ECSA values of 56.509 m^2/g (PTMPs 50 MEA), 56.215 m^2/g (PTMPs 500 MEA), 56.607 m^2/g (Bare MEA), and 56.262 m^2/g (NRE-211 MEA). This result indicated that all the MEAs were made with the same amount of catalyst and the embedded PTMPs did not affect the electrode property. Therefore, we can say that the performance enhancement of the PEMFC in high temperature and low humidity operating conditions is mainly ascribed to the water retention effect of the PTMPs by efficiently alleviating the dehydration of the membrane. Although this study has focused on the effect of surface-cover morphology of the porous TiO_2 filler

Table 3
Electrochemical surface area values extracted from Fig. S11.

ECSA	PTMPs 50 MEA	PTMPs 500 MEA	Bare MEA	NRE-211 MEA
m^2/g_{Pt}	56.509	56.215	56.607	56.262

with the fixed layer thickness, the thickness of the TiO_2 filler layer would be one of the critical factors determining the performance of the fuel cell. For this reason, we have tried to fabricate a membrane with a thicker TiO_2 filler layer with a diameter of 50 μm, denoted as PTMPs 50-T, by using the PUA stencil with a thickness of 40 μm and the fixed diameter of 50 μm (Fig. S12). As shown in Fig. S13 and Table S4, the MEA with the PTMPs-50 T showed much lower performances compared to those of the MEAs with PTMPs 50, PTMPs 500, and Bare membranes under all operating conditions. This result indicates that there is a constraint in the loading amount and thickness of the TiO_2 layer to obtain acceptable performances when designing PTMPs embedded membranes.

4. Conclusions

In this study, Nafion® composite membranes with patterned mesoporous TiO_2 microplates (PTMPs) (diameter of 50/500 μm and thickness of ~5.2 μm) were successfully developed via simple doctor blading method with polymeric micro-hole stencils and well-controlled auto-spray technique with Nafion® ionomer. This novel methodological approach effectively secured the proton transport pathway by resolving the agglomeration issue of the hygroscopic inorganic fillers when it is incorporated into the membrane as well as spatially locating the TiO_2 microplates on the surface of the membrane. The morphological and mechanical characteristics of the fabricated composite membranes were investigated and evaluated by comparing them to the bare spray-based membrane and the commercial Nafion® 211 membrane. Moreover, the electrochemical characteristics of the MEAs with those membranes were thoroughly investigated under various operating fuel cell operating conditions. Notably, under high temperature and low relative humidity condition (35% RH @120 °C), the PTMPs 50 MEA, with a diameter of ~50 μm and a height of ~5.2 μm, exhibited the maximum power density by more than 35.2% higher compared to that of the reference MEA. Indeed, much reduced ohmic and charge transport resistance were confirmed by the EIS measurement. The results indicated that the embedded hygroscopic mesoporous PTMPs play a role in attaining the water molecules at high temperature (>100 °C) and efficiently alleviating the membrane dehydration induced proton conductivity loss. This novel approach can provide a breakthrough for the operating of a high-temperature PEMFC and give an insight for fabricating organic/inorganic composite membrane with high fidelity and controllability.

CRediT authorship contribution statement

Le Vu Nam: Data curation, Funding acquisition, Investigation. **Eunho Choi:** Data curation, Funding acquisition, Methodology. **Segeun Jang:** Conceptualization, Writing – review & editing. **Sang Moon Kim:** Supervision, Writing – review & editing.

Declaration of competing interest

The authors declare that they have no known competing financial interests or personal relationships that could have appeared to influence the work reported in this paper.

Acknowledgment

This work was supported by the National Research Foundation (NRF) of Korea (NRF-2019R1C1C1004462, NRF-2019R1C1C1006392, and NRF-2021M3H4A1A02042957). This research was supported by Nano·Material Technology Development Program through the National Research Foundation of Korea(NRF) funded by the Ministry of Science, ICT and Future Planning (2009-0082580).

Appendix A. Supplementary data

Supplementary data to this article can be found online at https://doi.org/10.1016/j.renene.2021.08.062.

References

[1] M. Ball, M. Wietschel, The Hydrogen Economy: Opportunities and Challenges, Cambridge University Press, 2009.
[2] M. Aneke, M. Wang, Energy storage technologies and real life applications–A state of the art review, Appl. Energy 179 (2016) 350–377.
[3] P.P. Edwards, V.L. Kuznetsov, W.I. David, N.P. Brandon, Hydrogen and fuel cells: towards a sustainable energy future, Energy Pol. 36 (12) (2008) 4356–4362.
[4] J.-H. Wee, Applications of proton exchange membrane fuel cell systems, Renew. Sustain. Energy Rev. 11 (8) (2007) 1720–1738.
[5] T. Wilberforce, A. Alaswad, A. Palumbo, M. Dassisti, A.-G. Olabi, Advances in stationary and portable fuel cell applications, Int. J. Hydrogen Energy 41 (37) (2016) 16509–16522.
[6] S. Mekhilef, R. Saidur, A. Safari, Comparative study of different fuel cell technologies, Renew. Sustain. Energy Rev. 16 (1) (2012) 981–989.
[7] J. Larminie, A. Dicks, M.S. McDonald, Fuel Cell Systems Explained, J. Wiley Chichester, UK, 2003.
[8] R. O'hayre, S.-W. Cha, W. Colella, F.B. Prinz, Fuel Cell Fundamentals, John Wiley & Sons, 2016.
[9] F. De Bruijn, V. Dam, G. Janssen, Durability and degradation issues of PEM fuel cell components, Fuel Cell. 8 (1) (2008) 3–22.
[10] D. Chu, R. Jiang, Performance of polymer electrolyte membrane fuel cell (PEMFC) stacks: Part I. Evaluation and simulation of an air-breathing PEMFC stack, J. Power Sources 83 (1–2) (1999) 128–133.
[11] Y. Li, D.A. Dillard, Y.-H. Lai, S.W. Case, M.W. Ellis, M.K. Budinski, C.S. Gittleman, Experimental measurement of stress and strain in nafion membrane during hydration cycles, J. Electrochem. Soc. 159 (2) (2011) B173.
[12] J. Wu, X.Z. Yuan, J.J. Martin, H. Wang, J. Zhang, J. Shen, S. Wu, W. Merida, A review of PEM fuel cell durability: degradation mechanisms and mitigation strategies, J. Power Sources 184 (1) (2008) 104–119.
[13] S.J. Peighambardoust, S. Rowshanzamir, M. Amjadi, Review of the proton exchange membranes for fuel cell applications, Int. J. Hydrogen Energy 35 (17) (2010) 9349–9384.
[14] Y. Zhang, J. Li, L. Ma, W. Cai, H. Cheng, Recent developments on alternative proton exchange membranes: strategies for systematic performance improvement, Energy Technol. 3 (7) (2015) 675–691.
[15] S. Bose, T. Kuila, T.X.H. Nguyen, N.H. Kim, K.-t. Lau, J.H. Lee, Polymer membranes for high temperature proton exchange membrane fuel cell: recent advances and challenges, Prog. Polym. Sci. 36 (6) (2011) 813–843.
[16] S. Lee, S. Mukerjee, E. Ticianelli, J. McBreen, Electrocatalysis of CO tolerance in hydrogen oxidation reaction in PEM fuel cells, Electrochim. Acta 44 (19) (1999) 3283–3293.
[17] M. Schuster, T. Rager, A. Noda, K. Kreuer, J. Maier, About the choice of the protogenic group in PEM separator materials for intermediate temperature, low humidity operation: a critical comparison of sulfonic acid, phosphonic acid and imidazole functionalized model compounds, Fuel Cell. 5 (3) (2005) 355–365.
[18] M.K. Cho, H.-Y. Park, S.Y. Lee, B.-S. Lee, H.-J. Kim, D. Henkensmeier, S.J. Yoo, J.Y. Kim, J. Han, H.S. Park, Effect of catalyst layer ionomer content on performance of intermediate temperature proton exchange membrane fuel cells (IT-PEMFCs) under reduced humidity conditions, Electrochim. Acta 224 (2017) 228–234.
[19] M.A. Hickner, H. Ghassemi, Y.S. Kim, B.R. Einsla, J.E. McGrath, Alternative polymer systems for proton exchange membranes (PEMs), Chem. Rev. 104 (10) (2004) 4587–4612.
[20] Y. Devrim, H. Devrim, I. Eroglu, Polybenzimidazole/SiO2 hybrid membranes for high temperature proton exchange membrane fuel cells, Int. J. Hydrogen Energy 41 (23) (2016) 10044–10052.
[21] N. Shaari, S.K. Kamarudin, Recent advances in additive-enhanced polymer electrolyte membrane properties in fuel cell applications: an overview, Int. J. Energy Res. 43 (7) (2019) 2756–2794.
[22] G.G. Gagliardi, A. Ibrahim, D. Borello, A. El-Kharouf, Composite polymers development and application for polymer electrolyte membrane technologies—a review, Molecules 25 (7) (2020) 1712.
[23] S. Jang, Y.S. Kang, J. Choi, J.H. Yeon, C. Seol, M. Choi, S.M. Kim, S.J. Yoo, Prism patterned TiO2 layers/Nafion® composite membrane for elevated temperature/low relative humidity fuel cell operation, J. Ind. Eng. Chem. 90 (2020) 327–332.
[24] E. Chalkova, M.B. Pague, M.V. Fedkin, D.J. Wesolowski, S.N. Lvov, Nafion/ TiO2 proton conductive composite membranes for PEMFCs operating at elevated temperature and reduced relative humidity, J. Electrochem. Soc. 152 (6) (2005) A1035.
[25] Y. Jin, S. Qiao, L. Zhang, Z.P. Xu, S. Smart, J.C.D. da Costa, G.Q. Lu, Novel Nafion

composite membranes with mesoporous silica nanospheres as inorganic fillers, J. Power Sources 185 (2) (2008) 664–669.
[26] H. Thiam, W. Daud, S. Kamarudin, A. Mohammad, A. Kadhum, K. Loh, E. Majlan, Overview on nanostructured membrane in fuel cell applications, Int. J. Hydrogen Energy 36 (4) (2011) 3187–3205.
[27] R. Narducci, P. Knauth, J.-F. Chailan, M.L. Di Vona, How to improve Nafion with tailor made annealing, RSC Adv. 8 (48) (2018) 27268–27274.
[28] J. Li, X. Yang, H. Tang, M. Pan, Durable and high performance Nafion membrane prepared through high-temperature annealing methodology, J. Membr. Sci. 361 (1–2) (2010) 38–42.
[29] S. Pujiastuti, H. Onggo, Effect of various concentration of sulfuric acid for Nafion membrane activation on the performance of fuel cell, in: AIP Conference Proceedings, AIP Publishing LLC, 2016, 060006.